Lipopolysaccharide Bilayer Structure: Effect of Chemotype, Core Mutations, Divalent Cations, and Temperature†

Scott Snyder,‡ Dennis Kim,§ and Thomas J. McIntosh*,‡

Department of Cell Biology, Duke University Medical Center, Durham, North Carolina 27710, and Department of Mechanical Engineering, Duke University, Durham, North Carolina 27706

Received April 14, 1999; Revised Manuscript Received June 11, 1999

ABSTRACT: Lipopolysaccharide (LPS), the primary lipid on the surface of Gram-negative bacteria, is thought to act as a protective and permeability barrier. X-ray diffraction analysis of osmotically stressed LPS multilayers was used to determine the structure and interactive properties of LPSs from strains containing the minimum number of sugars necessary for bacterial survival (Re chemotype) to the maximum number of sugars found in rough bacteria (Ra chemotype). At 20 °C in the absence of divalent cations, LPS suspensions gave a sharp wide-angle reflection at 4.23 Å and a broad low-angle band centered at 50−68 Å depending on the chemotype, indicating the presence of gel phase bilayers separated by large fluid spaces. As osmotic pressure was applied, the apposing bilayers were squeezed together and lamellar diffraction at 6 Å resolution was obtained. At low applied pressures ($<10^6$ dyn/cm^2), the total repulsive pressure between bilayers could be explained by electrostatic double layer theory. At higher applied pressures, there was a sharp upward break in each pressure−distance relation, indicating the presence of a hydrophilic steric barrier whose range depended strongly on the LPS chemotype. The positions of these upward breaks, along with electron density profiles, showed that the sugar core width systematically increased from 10 Å for the Re chemotype to 27 Å for the Ra chemotype. In excess buffer, the addition of divalent cations brought the bilayers into steric contact. Electron density profiles were used to determine the locations of cation binding sites and polar substituents on the LPS oligosaccharide core. The area per hydrocarbon chain was approximately 26 Å^2 in liquid-crystalline LPS bilayers, an indication of an acyl chain packing that is much tighter than that found in bilayers composed of typical membrane lipids. This unusually tight packing could be a critical factor in the permeability barrier provided by LPS.

Unlike most types of cells, Gram-negative bacteria surround themselves with a double membrane (*1*, *2*). The outermost of these two membranes is asymmetric, with the inner monolayer composed of glycerophospholipids and the outer monolayer composed mostly of lipopolysaccharide (LPS)[1] (*2*−*4*). LPS is sometimes called endotoxin because of its toxic, inflammatory properties which can result in a potentially fatal phenomenon known as septic shock (*5*). A major function of this outer membrane is widely believed to be that of a protective barrier (*6*, *7*) which makes the bacteria resistant to a variety of host defense factors, including β-lysin, lysozyme, and various leukocyte proteins which are quite toxic to Gram-positive bacteria (*8*, *9*). In enteric bacteria such as *Escherichia coli*, this barrier acts to prevent the detergent action of bile salts (*2*). In addition, the outer membrane of Gram-negative bacteria acts as a barrier to the diffusion of many antibiotics, such as novobiocin, which are effective against other forms of bacteria. It has been argued that although hydrophilic antibiotics with a molecular mass of less than about 650 Da gain access to bacteria through aqueous pores in the outer membrane called porins (*10*), large hydrophobic molecules must pass through the bilayer itself to enter the cell. Apparently, LPS forms a very efficient barrier to the latter type of transport, as it has been shown that hydrophobic probe molecules permeate across the outer membrane at about 1−2% of the rates for typical phospholipid bilayers (*11*). Resistance of this sort can act in synergy with the resistance produced by antibiotic degrading enzymes and efflux pumps, allowing these mechanisms to work at much lower rates and still be effective (*7*).

Additional evidence for the role of LPS in the resistance of Gram-negative bacteria to hydrophobic molecules comes from comparisons of the properties of mutant rough and deep rough bacteria. The rough phenotype occurs when bacteria are unable to add a repeating tetrasaccharide to their outer core saccharide region, whereas deep rough bacteria are unable to attach the oligosaccharide core to the lipid A moiety (see Figure 1). In comparison to rough mutants, deep rough mutants lose their resistance to a number of hydrophobic antibiotics (*12*) and become more susceptible to detergents and lysozyme, and more permeable to steroids (*7*, *10*, *11*). Similarly, mutations in LPS structure which affect polar substituents on the core saccharides produce a phenotype similar to that of deep rough bacteria. Specifically, the rfaP$^-$ mutation, which renders the bacterium unable to attach

† This work was supported by Grants RO1 GM-27278, RO1 GM-58432, and T32 GM-08555 from the National Institutes of Health.

‡ Duke University Medical Center.

§ Duke University.

[1] Abbreviations: LPS, lipopolysaccharide; KDO, keto-*d*-octulosonic acid; PVP, poly(vinylpyrrolidone); PEG, poly(ethylene glycol).

10.1021/bi990867d CCC: $18.00
Published on Web 07/29/1999

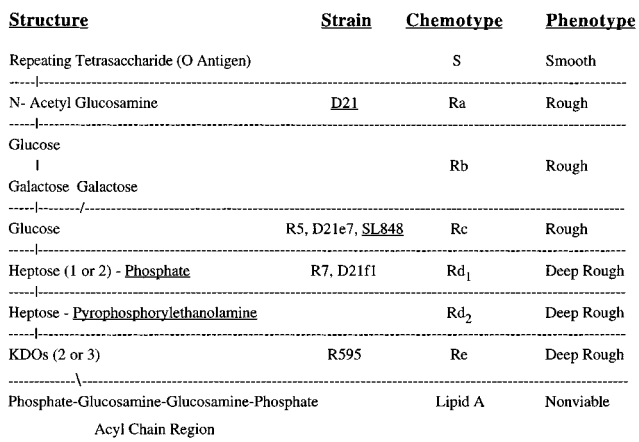

FIGURE 1: Generalized structure of LPS. The phenotype names (smooth and rough) refer to the appearance of bacterial colonies growing on agar plates. Lipid A contains a diglucosamine backbone, substituted on either side by phosphate groups, and an acyl chain region usually containing six or seven fatty acids. In general, the fatty acids are saturated and usually contain 14 carbons, although some contain 12 or 16 carbons. The "core" saccharide region of the LPS molecule extends from the lipid A moiety to the repeating tetrasaccharide (O antigen) region found in the smooth phenotype. The core contains two or three keto-*d*-octulosonic acids (KDOs) and a variable numbers of sugars, depending on the chemotype. The phosphate and pyrophosphorylethanloamine polar substituents on the inner core heptoses are only present in the underlined Ra and Rc strains.

phosphoethanolamine to the oligosaccharide core (Figure 1), increases susceptibility to novobiocin and detergents and retards the ability to grow on EMB agar (*13*, *14*). In addition, divalent cations have been shown both to decrease the hypersusceptibility of deep rough bacteria to antibiotics (*15*) and to decrease the permeability of LPS−lipid bilayers (*16*).

Thus, polysaccharide core mutations in LPSs have profound effects on microbial physiology and on susceptibility to various agents. Moreover, the aggregation state of these LPSs affects their bioactivity (*17*−*20*). Therefore, it is important to understand the structure, aggregation, and interactive properties of LPS. Previously, a number of X-ray diffraction studies with fully hydrated LPS suspensions have shown that specific LPSs can exhibit polymorphism and enter into nonbilayer phases under particular pH and ionic strength conditions (*21*−*23*). Superb, high-resolution X-ray patterns have also been obtained from partially hydrated LPS films (*24*−*26*), and modeling studies using energy minimization techniques have been performed (*22*, *24*, *27*). However, to date there has been relatively little rigorous Fourier analysis of the diffraction data, in part because of a lack of information about the phase angles of the intensity data. Moreover, there is little structural analysis of LPS in its liquid-crystalline phase.

In this paper, we use X-ray diffraction analysis of osmotically stressed LPS multibilayers to study the structure of both the hydrophilic barrier (provided by the oligosaccharide core) and the hydrophobic barrier (provided by the hydrocarbon chain region). The osmotic stress experiments provide diffraction data for tracing out the continuous Fourier transforms and determining the phase angle for each X-ray reflection so that electron density profiles can be calculated (*28*−*30*). We use these electron density profiles to determine the widths of the oligosaccharide and hydrocarbon regions of the bilayers. The profiles are also used to study the structural effect of loss of polar substituents conferred by the rfaP$^-$ mutation and to gain information about the location and nature of the binding of polyvalent cations to LPS bilayers. Pressure−distance relations obtained for LPSs from several chemotypes provide the range and magnitude of both the electrostatic pressure and the hydrophilic barrier provided by the polysaccharide region of the LPS molecules. In addition, the X-ray data are used to obtain the area per LPS hydrocarbon chain in the liquid-crystalline phase and to compare the packing properties of LPS molecules with typical membrane phospholipids.

MATERIALS AND METHODS

Materials. Lipopolysaccharide samples were either purchased from Sigma Chemical Co. (St. Louis, MO), as in the case of the *Salmonella minnesota* R595, R7, and R5, or extracted from bacteria, as in the case of *E. coli* D21, D21e7, and D21f1 and *Salmonella typhimurium* SL848 (see Figure 1). *E. coli* bacterial strains were obtained from J. A. Fralick (Texas Tech University Health Sciences Center, Lubbock, TX), and *S. typhimurium* SL848 was obtained from Salmonella Genetics Stock Center (Calgary, AB). LPS extractions were performed using the PCP extraction procedure of Galanos et al. (*31*) with the acetone precipitation and ethanol washing procedures of Qureshi et al. (*32*). Briefly, ether powders of ethanol-extracted cells were extracted with 2:5:8 (v/v/v) phenol/chloroform/petroleum ether and then centrifuged to remove unwanted material. The extraction solution was then dried with a rotary evaporator to remove chloroform. Acetone and diethyl ether were subsequently added to precipitate LPS.

To ensure that our isolated LPS was in a single, defined salt form, we used an EDTA/HCl washing procedure. The LPS, in a solution of 20 mM triethylammonium EDTA (pH 7.0), was sonicated in a bath sonicator and extracted with 2.5 volumes of 2:1 chloroform/methanol. The solution was then vortexed and centrifuged as necessary to enhance separation of the aqueous and organic phases, and the organic phase was transferred to fresh tubes with 0.4 volume of methanol and 0.6 volume of 0.1 N HCl. This organic phase was then vortexed and centrifuged as described above. The aqueous phases from both the EDTA and HCl washing steps were subsequently processed with the same procedures, and the combined organic phases were dried under nitrogen. The LPS was then resuspended in 20 mM Hepes buffer (pH 7.0) containing either 100 mM NaCl (for the sodium salt form) or 100 mM NaCl with 10 mM $CaCl_2$, $BaCl_2$, $MgCl_2$, $MnCl_2$, or $Co(NH_3)_6Cl_3$ (for the calcium, barium, magnesium, manganese, or cobalt hexamine salt forms, respectively). Thorough mixing of the salts and the LPS was achieved by several freeze−thaw cycles.

Osmotic Stress and X-ray Diffraction Experiments. Two types of lipid systems were examined by X-ray diffraction, unoriented suspensions and oriented multilayers. Known osmotic pressures were applied to both of these systems by published procedures (*30*, *33*−*35*). To prepare unoriented suspensions, LPS was dried from the organic phase under nitrogen and incubated with periodic vortexing for several hours at 60 °C in the buffered solutions (listed above) containing various concentrations of the neutral polymers poly(vinylpyrrolidone) (PVP) and dextran. For all of these

LPSs, 60 °C is above the lipid phase transition temperature, which is between 30 and 37 °C (*36*). Several freeze−thaw cycles were used to ensure that the salts were uniformly distributed throughout the multilayers. Since dextran or PVP is too large to enter the lipid lattice, it competes for water with the lipid multilayers, thereby applying an osmotic pressure (*33*, *34*). Values of osmotic pressures for these polymer solutions have been published (*37*). The lipid suspensions were sealed in quartz X-ray capillary tubes and mounted in a temperature-controlled chamber in a point-collimator X-ray camera.

To prepare oriented multilayers, the LPS/buffer suspensions were first washed (to remove excess salt) by pelleting the appropriate suspensions with a bench centrifuge, suspending in water, repelleting, and resuspending in water. A drop of the LPS/water suspension was dried onto a curved glass substrate. The multilayers on the substrate were mounted in a temperature-controlled humidity chamber on a single-mirror (line-focused) X-ray camera such that the X-ray beam was oriented at a grazing angle relative to the multilayers (*35*, *38*). Pressures were applied to the oriented multibilayers by incubating them in constant relative humidity atmospheres maintained with saturated salt solutions. To speed equilibration, a gentle stream of nitrogen was passed through a flask of the saturated salt solution and then through the chamber. The ratio of the vapor pressure (p) of various salt solutions to the vapor pressure of pure water (p_o) has been determined (*39*, *40*). The applied pressure is given by

$$P = -(RT/V_w) \times \ln(p/p_o) \quad (1)$$

where R is the molar gas constant, T is the temperature in kelvin, and V_w is the partial molar volume of water (*34*).

X-ray diffraction patterns were recorded at temperatures of either 20 or 50 °C on Kodak DEF X-ray film. X-ray films were processed by standard techniques and densitometered with a Joyce-Loebl microdensitometer as described previously (*30*, *35*, *38*, *41*). After background subtraction, integrated intensities, $I(h)$, were obtained for each order h by measuring the area under each diffraction peak. For unoriented patterns, the structure amplitude $F(h)$ was set equal to $[h^2I(h)]^{1/2}$ (*42*, *43*). For the oriented line-focused patterns, the intensities were corrected by a single factor of h due to the cylindrical curvature of the multilayers (*42*, *43*) so that $F(h) = [hI(h)]^{1/2}$. Electron density profiles, $\rho(x)$, on a relative electron density scale were calculated from

$$\rho(x) = \left(\frac{2}{d}\right) \sum \exp[i\phi(h)] \times F(h) \times \cos\left(\frac{2\pi x h}{d}\right) \quad (2)$$

where x is the distance from the center of the bilayer, d is the lamellar repeat period, $\phi(h)$ is the phase angle for order h, and the sum is over h. Phase angles were determined by using the sampling theorem (*29*, *44*, *45*) as described previously (*30*, *38*, *46*). Electron density profiles described in this paper are at a resolution $d/2h_{max}$ of ≈6 Å.

RESULTS

X-ray Diffraction and Osmotic Stress Experiments. At 20 °C and in the absence of applied pressure, suspensions of LPS bilayers in their sodium salt form gave X-ray diffraction patterns which had a single sharp wide angle band at 4.23 Å and a broad low-angle band. The spacing of the low-angle band depended on the LPS chemotype. The centers of the band were at spacings of approximately 65, 68, 60, and 50 Å for Ra, Rc, Rd, and Re LPS, respectively (Table 1). When osmotic pressure was applied, either by the addition of PVP or by equilibration in a controlled humidity atmosphere, the low-angle pattern consisted of a series of sharp reflections that were indexed as orders of a lamellar repeat period. Such patterns are consistent with well-ordered stacks of lipid bilayers (*47*). For all the LPS molecules that were tested, the repeat period decreased with increasing osmotic pressure (Figure 2) while the wide-angle reflection remained unchanged.

Table 1: Diffraction Data for LPS Bilayers in the Presence and Absence of Polyvalent Cations with No Applied Pressure[a]

chemotype	strain/mutation	cation	wide-angle spacings (Å)	lamellar repeat period
Rd	mR7/rfaP$^-$	Na^+	4.23	none, band at ≈60 Å
	mR7/rfaP$^-$	Mg^{2+}	4.23	69.6 Å
	mR7/rfaP$^-$	Ba^{2+}	4.23	70.6 Å
Rc	SL848/rfaP$^+$	Na^+	4.23	none, band at ≈68 Å
	SL848/rfaP$^+$	Mg^{2+}	4.28, 4.10, 3.69	77.0 Å
	SL848/rfaP$^+$	Mn^{2+}	ND[b]	79.2 Å
	SL848/rfaP$^+$	$Co(NH_3)_6^{3+}$	ND	75.3 Å
	R5/rfaP$^-$	Mg^{2+}	4.23	88.6 Å
	D21e7/rfaP$^-$	Mg^{2+}	ND	82.5 Å
Ra	D21/rfaP$^+$	Na^+	ND	none, band at ≈65 Å
	D21/rfaP$^+$	Mg^{2+}	4.23	110 Å
	D21/rfaP$^+$	Ca^{2+}	ND	110 Å
	D21/rfaP$^+$	Ba^{2+}	ND	104 Å

[a] Measurements were taken at 20 °C in an aqueous solution of 20 mM Hepes buffer (pH 7.0). Experiments with polyvalent cations contained a ≥30-fold molecular ratio of cation to LPS. [b] Not detected.

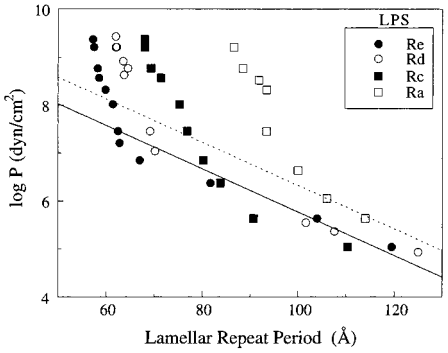

FIGURE 2: Plot of the logarithm of applied osmotic pressure (log P) vs the lamellar repeat period for LPS from mutant chemotypes Ra (*E. coli* D21), Rc (*S. minnesota* R5), Rd (*S. minnesota* R7), and Re (*S. minnesota* R595). For the Rc chemotype, similar pressure−distance data were obtained from LPS isolated from the D21e7 strain (data not shown). The solid line represents expected electrostatic repulsion between adjacent Rc, Rd, or Re bilayers as calculated from double layer theory (see the text for details), whereas the dotted line is the calculated electrostatic pressure for Ra LPS which has additional charges due to the presence of the polar substituents in the saccharide core (Figure 1).

At applied osmotic pressures (P) from 1×10^4 to 1×10^6 dyn/cm^2 ($4 < \log P < 6$), the repeat periods decreased such that values of log P versus d for all LPSs fell close to a straight line. The solid and dotted lines in Figure 2 correspond to the calculated repulsive pressure between charged LPS bilayers of the different chemotypes as predicted by

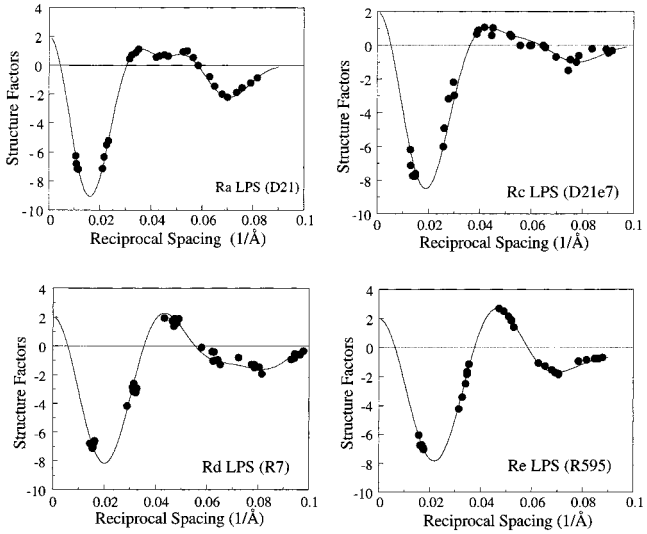

FIGURE 3: X-ray diffraction structure factors plotted vs reciprocal space coordinates for osmotic pressure experiments with LPSs from Ra, Rc, Rd, and Re mutants. In each panel, the solid line corresponds to the continuous Fourier transform of the unit cell as calculated from the sampling theorem (see the text for details).

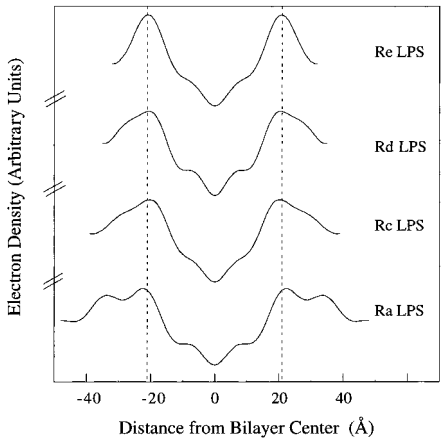

FIGURE 4: Electron density profiles of LPSs from Ra (D21), Rc (D21e7), Rd (R7), and Re (R595) mutants at the same osmotic pressure (log $P = 7.5$). In each profile, the low-density dip in the center corresponds to the localization of the terminal methyl groups, the high-density peaks at ±21 Å (denoted by vertical dotted lines) correspond to the high-density headgroups of the lipid A, and the medium-density regions at the outer edges of the profile correspond to the saccharide region of the molecule. The lipid A portion of each chemotype has approximately the same width, whereas the width of the saccharide region systematically increases from Re to Rd to Rc to Ra.

double layer theory (*48*) (see the Discussion for details). At higher applied pressures (log $P > 6$), there were sharp upward breaks in the pressure−distance relations, with the position of the upward break depending on the type of LPS; the upward breaks from the dotted line appeared at repeat periods of approximately 95, 82, 70, and 62 Å for Ra, Rc, Rd, and Re LPSs, respectively. Our repeat periods for Re LPS for the higher applied pressures were slightly smaller than those recorded by Nauman et al. (*22*) for the triethylamine salt form of *S. minnesota* mR595 LPS over a similar range of relative humidity atmospheres, and our repeat periods at the highest applied pressures were quite similar to those recorded by Kastowsky et al. (*26*) for "dry" LPSs from Ra, Rc, Rd, and Re chemotypes.

Fourier Analysis of Low-Angle Diffraction. Structure factors for osmotic stress and X-ray diffractions experiments are shown in Figure 3. Note that for each LPS that was studied the structure amplitudes fell on a smooth curve (solid line in each panel of Figure 3) that represents the continuous Fourier transform of the bilayer electron density profile (*29*, *30*). The solid lines in Figure 3 were calculated with the sampling theorem (*29*, *44*−*46*) for one data set for each LPS with the phase angle for each reflection that gave the best fit to the rest of the diffraction data. As noted above, in the sodium salt form of each LPS that was studied the diffuse low-angle bands observed in the absence of applied pressure were at spacings between 68 and 50 Å (reciprocal spacings of 0.015−0.020 $Å^{-1}$) which correspond to the position of the first negative peak of the respective continuous transforms (Figure 3). Thus, the low-angle band observed in excess buffer is consistent with the presence of bilayers with a large, indefinite swelling between the bilayers (*29*, *30*).

Using these structure amplitudes (Figure 3), we have calculated electron density profiles for the Ra, Rc, Rd, and Re LPS chemotypes (Figure 4). For each profile, the center of the bilayer was placed at the origin. There were several common features to the profiles. First, for each LPS chemotype, there was a very similar electron density distribution near the center of the profile. At the center of each profile was a dip in electron density which corresponds to the terminal methyl groups of the fatty acid chains. For each profile, the highest density peaks were at approximately the same location (±21 Å), denoted by vertical dotted lines. These electron density peaks correspond to the location of the high-density phosphate groups in the lipid A moiety. The medium-density regions of the profile, located between the terminal methyl trough at the center of the profile and the high-density headgroup peaks, correspond to the methylene groups of the lipid hydrocarbon chains. The central regions of these profiles (between the dotted lines) were very similar in appearance to the hydrocarbon regions of profiles of gel phase phospholipid bilayers (*30*, *47*, *49*−*51*). In contrast, the electron density distributions outside the dotted lines were quite different for the different LPS chemotypes. Specifically, the width of the medium-density region at the outer edges of the profiles increased in going from Re to Rd to Rc to Ra LPS, reflecting the increasing number of sugars in the oligosaccharide cores of these molecules (see Figure 1). Interestingly, the Ra LPS exhibited additional peaks in the electron density profile (at ±32 Å), which as described below, correspond to the phosphorylated heptose regions of this chemotype.

Structure of LPSs from Polar Substituent Mutations. To examine further the effect of polar substituent mutations on the electron density profiles of LPS, we have determined electron density profiles for the Rc chemotype of LPS in both its $rfaP^+$ and $rfaP^-$ forms. The rfaP allele is thought to be involved in the addition of polar substituents (phosphate and pyrophosphorylethanolamine) to the heptose region of the LPS molecule, as mutants lacking this allele have LPS which lacks these polar moieties (*13*). Figure 5 shows diffraction analysis from two Rc LPS samples, one from an $rfaP^+$ strain, *S. typhimurium* SL848, and the other from an $rfaP^-$ strain, *E. coli* D21e7. The structure factors (Figure 5A) for the D21e7 and SL848 strains were similar, but not identical. For example, for reciprocal spacings from 0.07 to

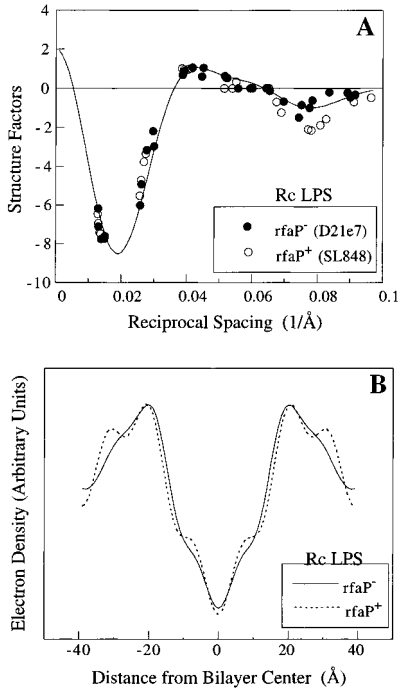

FIGURE 5: X-ray diffraction analysis of rfaP$^-$ (R5) and rfaP$^+$ (SL848) polar substituent mutations of Rc chemotypes: (A) structure factors and (B) electron density profiles. In panel A, the solid line is the continuous transform of the rfaP$^-$ data. In panel B, the profiles are similar for the lipid A core of each molecule. However, the rfaP$^+$ profile has additional high-electron density peaks centered at approximately ±31 Å which correspond to the heptose polar substituents.

0.08 Å^{-1}, the structure factors for the SL848 fell well below the continuous transform of D21e7 (solid line in Figure 5A). Electron density profiles of SL848 and D21e7 (Figure 5B) had similar hydrocarbon regions and high electron density peaks at ±21 Å. However, the profile of SL848 LPS had additional high-density peaks at ±31 Å, indicating the presence of the high-electron density phosphate and pyrophosphorylethanolamine groups on the saccharide chains (see Figure 1).

Structural Effects of Divalent Cations. Table 1 compares both the wide-angle and low-angle spacings of LPS in the presence and absence of divalent cations. For Ra and Rd LPS, the wide-angle patterns were not measurably modified by the presence of divalent cations. However, for Rc SL848 LPS the sodium salt form gave a single sharp band at 4.23 Å, whereas the magnesium salt form gave three sharp and distinct wide-angle reflections at 3.69, 4.10, and 4.28 Å, consistent with a change from a hexagonal chain packing arrangement of the hydrocarbon chains in the sodium salt form to a nonhexagonal arrangement in the magnesium form. In excess buffer, in the absence of applied pressure, the presence of divalent cations converted the broad low-angle bands to sharp reflections that were indexed as multiple orders of lamellar repeat periods. The repeat period depended on the LPS chemotype (Table 1). Our observed repeat periods in the presence of divalent cations in excess buffer were somewhat larger than those obtained by Labischinski et al. (*23*) for various rough mutant LPSs at a 1:1 cation:LPS ratio in 70% water. For each chemotype, the observed lamellar spacing was similar to the spacing recorded where the upward break in the pressure−distance curve was observed with the sodium salt forms under applied osmotic pressure

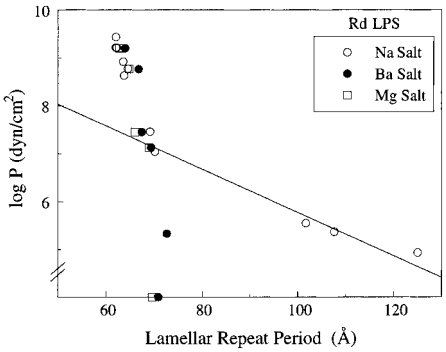

FIGURE 6: Lamellar repeat periods as a function of applied pressure for the sodium, barium, and magnesium salt forms of Rd (R7) LPS. The data points on the *x*-axis for the barium and magnesium salt forms correspond to repeat periods obtained in the absence of applied osmotic pressure. The solid line represents the expected electrostatic repulsion between LPS bilayers in 100 mM NaCl (see Figure 2).

(Figure 2). This reduction of the fluid space between bilayers was seen with the group 2 metal cations magnesium, calcium, and barium salts, as well as with $Co(NH_3)_6$ (Table 1). With applied pressures of $>10^7$ dyn/cm^2 (log $P > 7$), the repeat periods for both R7 (Figure 6) and D21 LPS (data not shown) were virtually unchanged by the addition of divalent cations.

To determine where divalent cations bound to the LPS bilayer, we performed a Fourier analysis of diffraction data obtained from oriented multilayers. Figure 7A shows the structure amplitudes and continuous transforms of Ra (D21) LPS in the sodium and barium salt forms. The structure factors were similar, but differed in the region of the transform near 0.03 Å^{-1}. Figure 7B shows electron density profiles for D21 LPS in the sodium and barium salt forms for three osmotic pressure values. For each salt form, the shape of the profile did not appreciably change with increasing osmotic pressure. However, the shape of the high-density regions of the profiles was altered by the addition of barium (Figure 7B). As barium is more electron dense than sodium, we would expect to see an increase in the electron density profile in the regions where the divalent cations bound. To put the profiles in the presence and absence of barium on the same relative electron density scale, we used the continuous transform data from oriented specimens to provide information about the density of the fluid regions between bilayers. Since the LPS bilayers were washed in water before equilibration in the relative humidity atmospheres, the electron density of the fluid layers between bilayers should be similar. The continuous transforms were used to generate structure factors for bilayers with an invented repeat period of 200 Å, and the profiles of the sodium and barium salt forms were then superimposed by matching the densities of the profiles in both the bilayer hydrocarbon region and the large fluid space between bilayers (Figure 7C). It can be seen that there was an increased electron density in the high-density region of the bilayer, most noticeably between the inner high-density peaks corresponding to the lipid A phosphates (at ±21 Å) and the outer high-density peaks corresponding to the phosphate and pyrophosphorylethanolamine substituents (at ±32 Å). That is, it appears that the barium primarily bound near the keto-*d*-octulosonic acid (KDO) residues of the inner core (Figure 1).

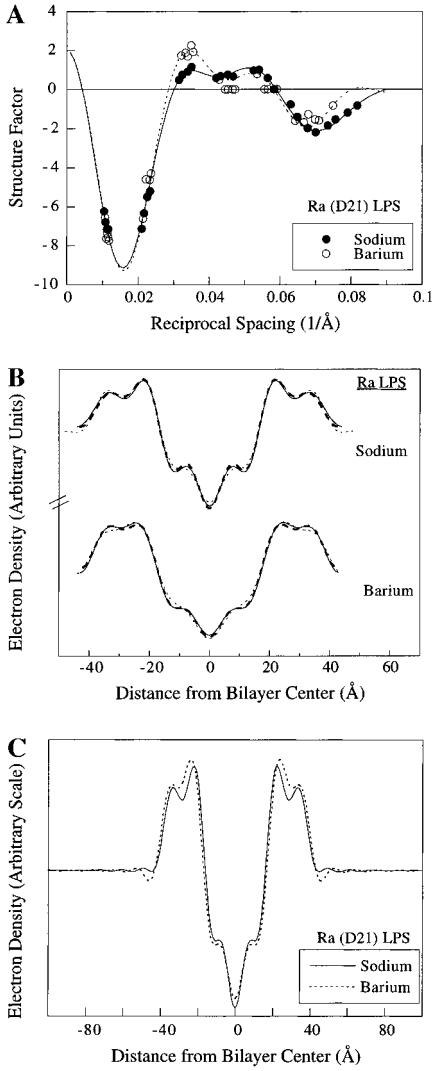

FIGURE 7: X-ray diffraction analysis of Ra (D21) LPS in the presence of NaCl and $BaCl_2$. Panel A shows the structure factors for the sodium (●) and barium salt forms (○) as well as the continuous transforms for the sodium salt form (solid line) and barium salt form (dashed line). Panel B shows electron density profiles for each salt form for a range of applied osmotic pressures (dotted lines correspond to a log *P* of 8.3, solid lines to a log *P* of 8.8, and dashed lines to a log *P* of 9.2). Panel C presents superimposed electron density profiles obtained from Fourier analysis of the continuous transforms shown in panel A (see the text for details). In panel C, the electron density profiles from the two salt forms superimpose quite closely in the lipid A regions of the profiles (from −20 to ±20 Å) and for the fluid spaces between bilayers (at the edges of each profile, from −40 to −100 Å and from 40 to 100 Å). However, the barium salt form has a higher electron density in the saccharide regions of the bilayer (between −20 and −40 Å and between 20 and 40 Å).

Liquid-Crystalline Phase Structure. The structures of the gel and liquid-crystalline phases were compared for the sodium and magnesium salt forms of Rd (R7) and Rc (SL848) LPSs. The gel to liquid-crystalline phase transition temperatures for Rd and Rc chemotypes of LPS range between 29 and 34 °C (*23*). As noted above, at 20 °C the wide-angle pattern consisted of a sharp reflection at 4.23 Å, whereas at 50 °C the wide-angle pattern consisted of a broad band at 4.5 Å, consistent with a liquid-crystalline phase (*47*). At 50 °C two orders of a lamellar repeat period were recorded for each LPS sample. Table 2 shows the repeat periods for gel and liquid-crystalline phases obtained at a constant applied pressure ($P = 0$ dyn/cm^2 for the magnesium salt form of Rc LPS and $P = 1.5 \times 10^7$ dyn/cm^2 for the sodium salt form of Rc and both the sodium and magnesium salt forms of Rd LPS). For all of these specimens, the lamellar repeat period decreased about 5 Å in going from the gel to liquid-crystalline phase. Control experiments showed that this change was reversible, as the original gel phase lamellar repeat period and wide-angle spacing were obtained after recooling the specimen to 20 °C.

Table 2: Lamellar Repeat Periods for Gel and Liquid-Crystalline Phases[a]

			repeat period		
strain	chemotype	salt	22 °C	50 °C	change in repeat period
R7	Rd P^-	Na	68.2	62.8	5.4
R7	Rd P^-	Mg	68.8	63.7	5.1
SL848	Rc P^+	Na	78.8	74.4	4.4
SL848	Rc P^+	Mg	79.7	74.7	5.0

[a] All buffers contained 100 mM NaCl and 20 mM Hepes (pH 7.0). For the sodium salt form, the buffer also contained 39.5% PVP which provided a constant osmotic pressure. The magnesium salt form buffer contained 10 mM $MgCl_2$.

DISCUSSION

The results presented in this paper provide direct information about the structure of bilayers of LPS isolated from various chemotypes and about the interactive properties of these bilayers.

LPS Aggregation State. The wide-angle and low-angle diffraction data show that at neutral pH both monovalent and multivalent salt forms of LPS were organized into gel phase bilayers at room temperature and liquid-crystalline phase bilayers at 50 °C. In the presence of applied osmotic pressure, or in the presence of divalent cations (Figures 2 and 6 and Tables 1 and 2), lamellar (bilayer) diffraction was observed for all the LPSs that were studied. The broad low-angle band observed for the sodium salt form of each LPS in the absence of applied pressure (Table 1) is also consistent with a bilayer phase, as each band was observed at the position of the first peak in the continuous transform of the bilayer (Figure 3). Brandenburg, Seydel, and colleagues (*23*, *52*) have studied the polymorphism of several LPSs under a range of temperatures and divalent cation concentrations. They observed diffraction patterns which are consistent with both lamellar and nonlamellar structures, with the nonlamellar structures being observed primarily at relatively high temperatures above the phase transition and with large magnesium concentrations. One discrepancy between our data and theirs is that for LPS from *S. minnesota* strain R595 at 20 °C they (*52*) recorded diffraction consistent with a lamellar phase for 1:1 LPS:Mg^{2+}, but a cubic phase for LPS in 80% water. We have not observed reflections consistent with a cubic phase with this LPS for the large range of buffer contents we have studied.

LPS Bilayer Structure. For each LPS that was studied, the osmotic stress experiments have allowed us to control the fluid spacing between the bilayers, and therefore use the "swelling method" (*28*−*30*) to trace the continuous Fourier transform of the LPS bilayer (Figure 3) and rigorously assign phases to the X-ray reflections. The resulting electron density profiles (Figures 4, 5B, and 7B) were calculated at moderate

resolution ($d/2h_{max} \approx 6$ Å). For each LPS chemotype, the phase angles determined by this analysis were consistent with all of the osmotic stress diffraction data. Moreover, the similarity of the hydrocarbon regions of the profiles from the different chemotypes (Figure 4) provides additional verification of the correctness of these phase combinations.

Our profiles for Re and Rd LPS (Figure 4) were similar to those reported for these LPSs by Kastowsky et al. (*26*), whereas our profiles for Ra LPS were at a much higher resolution than those of Kastowsky et al. (*26*), who were only able to record 2−3 orders of diffraction from this lipid. We found that the EDTA washing procedure markedly improved the quality (resolution) of our diffraction patterns for this lipid.

The wide-angle data and electron density profiles provide complementary information about the packing and orientation of the lipid A hydrocarbon chains. In the sodium salt form, the wide-angle spacing was the same for each chemotype, with the sharpness of the reflection indicating that the hydrocarbon chains were oriented approximately perpendicular to the bilayer plane (*47*). For all gel phase LPS bilayers, Ra, Rc, Rd, and Re chemotypes, the distance between the lipid A phosphate peaks in the electron density profile was about 42 Å. The following calculation shows this headgroup peak separation is consistent with the gel phase hydrocarbon chains being oriented perpendicular to the plane of the bilayer. The length of a gel phase hydrocarbon chain containing 14 carbons is 14 × 1.25 Å (17.5 Å), meaning that the thickness of the hydrocarbon region of gel phase LPS with untilted hydrocarbon chains should be about 35 Å. Single crystals of FhuA, the receptor for ferrichrome iron in *E. coli*, contain a single LPS molecule (*53*) which shows that the distance between the initial carbonyl carbon and the center of the phosphorylated glucosamine is 3−4 Å. Therefore, if it is assumed that the hydrocarbon chains are oriented perpendicular to the plane of the bilayer, the distance between the lipid A headgroup peaks across the bilayer is expected to be 41−43 Å, in agreement with our measured value of 42 Å.

As determined from the electron density profiles (Figure 4) and the pressure−distance relations (Figure 2), the oligosaccharide core length systematically increased on going from Re to Ra chemotypes. That is, the distance between the phosphate groups in the lipid A core (high-density peaks at ±21 Å in Figure 4) and the outer edge of the polysaccharide core increased on going from Re to Rd to Rc to Ra LPS (Figure 4). As described below, the pressure−distance relations can be used to obtain accurate estimates for the total bilayer width.

Effects of Polar Mutations. Polar mutations have minimal effect on the polysaccharide core width of Rc LPS as both R5 (Rc rfaP$^-$) and SL848 (Rc rfaP$^+$) have very similar total widths at the same osmotic pressures (Figure 5B). As the rfaP mutation confers an antibiotic sensitive phenotype, this suggests that core width by itself plays little role in conferring decreased permeability to these bilayers or antibiotic resistance to their parent organisms.

The polar substituents alter the bilayer electron density profile by adding peaks of electron density approximately 31 Å from the center of the bilayer (Figure 5B). This is in good agreement with molecular models for the location of the second heptose residue in the inner core (*26*, *27*).

Interactions between LPS Bilayers. LPS molecules contain a number of charged groups, including the phosphates of the lipid A moiety, the carboxylates of the KDO moieties, and phosphates attached to the heptose sugars in the inner core region for Ra, Rb, and some Rc and Rd strains (see Figure 1). Therefore, in excess buffer one expects that there should be electrostatic repulsion between LPS bilayers. The electrostatic repulsive pressure between two planar, charged surfaces at constant surface potential is given by

$$P_{es} = (64kT)c\gamma^2 \times \exp(-KD) \qquad (3)$$

where T is temperature, c is the bulk electrolyte concentration, $\gamma = \tan h(e\psi_o/4kT)$ where ψ_o represents the membrane surface potential, K is the Debye length, and D is the distance between the planes where the charges are located (*48*). For 100 mM NaCl buffer, $K = 1/(9.6$ Å) and ψ_o can be evaluated from the Gouy−Chapman equation, $\sin h(\psi_o/51.4$ mV) [$=136\sigma/\sqrt{c}$, where σ is the surface charge density (in e$^-$/Å^2)]. For LPS bilayers, the calculation of P_{es} is complicated by the fact that there are several charged groups located at different planes in the bilayer. For example, at pH 7, it has been shown that Re LPS is tetraanionic (*54*), with one negative charge for each phosphate group in the LPS moiety and one negative charge for each KDO carboxylate (see Figure 1). We assume that all of the LPSs studied in this paper have these four negative charges. In addition, Rc (SL848) and Ra (D21) LPS have two additional negative charges due to the phosphate and pyrophosphorylethanolamine polar substituents on the sugar core (Figure 1). Note that several of the LPSs that we have studied, including Rd (R7) and Rc (R5 and D21e7), are rfaP$^-$ and therefore do not have these charged heptose substituents. Thus, for Re, Rd (R7), and Rc (R5 and D21e7) LPS, we assume that there are two charged planes (each with two charges per LPS molecule), one going through the phosphate groups in the lipid A moiety and the second going through the KDO groups, whereas for Ra and Rc (SL848) we assume that there is an additional charged plane going through the phosphate and pyrophosphorylethanolamine groups on the sugar core. To estimate the location of these planes, we use the electron density profiles (Figures 4 and 5B). To calculate σ for each of these planes of charge, we first use the wide-angle diffraction spacing ($d_s = 4.23$ Å) to estimate the area per LPS molecule. The area per hydrocarbon chain in the gel phase, calculated from $A_g = 2(d_s)^2/(3)^{1/2}$ (*47*), is 20.7 Å^2. Assuming seven hydrocarbon chains per LPS molecule, we calculate an area per molecule of 145 Å^2. (We note that some of the strains used may have either six or seven hydrocarbon chains per molecule. However, that difference would have a relatively small effect on the calculated electrostatic pressure.) Therefore, for each of the three planes (through the lipid A phosphates, the KDOs, and the phosphate and pyrophosphorylethanolamine located on the sugar core), we estimate a σ of 2/(145 e$^-$/Å^2) (=0.014 e$^-$/Å^2). With these assumptions, we use eq 3 to estimate the total electrostatic repulsive pressure for Re, Rd rfaP$^-$ (R7), and Rc rfaP$^-$ (R5 and D21e7) LPSs (solid line in Figure 2) and for Ra and Rc rfaP$^+$ (SL848) LPSs (dotted line in Figure 2). For low applied pressures ($\log P < 6.5$), the observed pressure−distance data points fell quite close to the appropriate calculated electrostatic repulsion (Figure 2).

As observed for other bilayer systems (*46*, *55*), for each LPS at high applied pressures (log $P > 6.5$), there was an upward break in the pressure−distance relation from the expected electrostatic pressure line (Figure 2). These upward breaks represent the onset of steric pressure between apposing bilayer surfaces (*35*, *38*, *46*, *55*). Therefore, the positions of the upward breaks provide estimates for the total width of a single hydrated LPS bilayer: 95, 82, 70, and 62 Å for Ra, Rc, Rd, and Re LPS, respectively. These widths are somewhat larger than the estimates of bilayer widths of 88, 72, 70, and 56 Å for Ra, Rc, Rd, and Re LPS, respectively, obtained from repeat periods of LPS in water-saturated air (*26*, *27*). However, as noted by Kastowsky et al. (*26*), their experimental values were somewhat smaller than those expected from molecular model calculations. Thus, we argue that the position of the upward break in the pressure−distance curve probably provides a somewhat more accurate estimate for the total width of the LPS bilayer than that given by a repeat period measured under conditions where the polysaccharide cores from apposing bilayers might be compressed or have interpenetrated.

It is interesting to compare the properties of the steric barrier of the oligosaccharide core of LPS to the barrier provided to liposomes by the addition of lipids with covalently attached poly(ethyleneglycol) chains. Such PEG liposomes are being developed for drug delivery applications because the steric barrier provided by the PEG extends the blood circulation time of the liposome (*56*−*58*). Moreover, it has been found that the incorporation of 20 mol % PEG/lipid with a PEG molecular weight of 750 inhibits the partitioning of lysophosphatidylcholine micelles (but not monomers) into the bilayer (*59*). That is, the PEG steric barrier acts as a molecular "filter" and stabilizes the bilayer from a solution of lysophosphatidylcholine that would otherwise dissolve it (*59*). Our data (Figures 2 and 4) show that the range of the steric barrier of Ra LPS was greater than observed for liposomes containing 20 mol % PEG-750 [see Figure 5 of Kenworthy et al. (*60*)]. Thus, the steric barrier provided by this LPS saccharide core could help protect the bacterial membrane from the action of detergent micelles.

The pressure−distance relations, together with the electron density profiles, can be used to give accurate estimates for the width of the sugar core regions for each LPS. Subtraction of the peak-to-peak distance (42 Å) in the profiles from the total bilayer width (as determined above from the pressure−distance relations) gives the width of the polysaccharides extending from both sides of the bilayer. Therefore, as measured from the phosphate moieties in the lipid A backbone, the saccharides extend about 27, 20, 14, and 10 Å for Ra, Rc, Rd, and Re LPS, respectively.

Effects of Divalent Cations on LPS Structure and Interactive Properties. The addition of divalent cations to LPS suspensions modified the wide-angle and low-angle diffraction spacings (Table 2) as well as the pressure−distance relation (Figure 6). The changes in the wide-angle diffraction, only observed with SL848 LPS, indicate that the divalent cations changed the in-plane packing of these LPS molecules, converting the hydrocarbon chain packing from a hexagonal to a nonhexagonal lattice. The electron density profiles (Figure 7C) indicate that barium added density to the region of the profile located in the inner sugar core region, primarily near the KDO moieties. Although the changes in the profiles were small with the addition of barium, they were quite reproducible and were seen at all osmotic pressures (Figure 7B). Therefore, the divalent cations bound primarily to this region of the molecule, a result consistent with the results of Schindler and Osborn (*61*). The observed changes in the low-angle diffraction (Table 1 and Figure 6) indicate that the divalent cations collapsed the fluid space between apposing bilayers. That is, in the presence of divalent cations, but in the absence of applied pressure, the lamellar repeat period was similar to that recorded for LPS in the sodium salt under osmotic stresses large enough to bring apposing bilayers into steric contact (Figures 2 and 6). Although some authors (*10*) have suggested that multiple LPS molecules may chelate to a single divalent cation producing a series of intermolecular cross-bridges, these reduced lamellar repeat periods are unlikely to be a result of this phenomenon for several reasons. First, the effect is noted for all the LPS chemotypes that were tested, and the divalent cation binding seems to be primarily in the inner core region. Although interbilayer cross-bridging by divalent cations might be possible for Re LPS where the inner core is near the edge of the LPS molecule, it is difficult to imagine how two bilayers of the Ra chemotype could be cross-linked by a single metal ion since there would be a total of at least 20 Å of core width between their respective inner core regions. Further, cobalt hexamine produced an effect similar to that of the group II metals (Table 1) even though its inner coordination sphere is completely substituted with ammonia groups which cannot be displaced by groups on the LPS molecule (*62*). This indicates that a tight complex involving the displacement of water from the inner coordination shell of the divalent cation is not required for the observed reduction of interbilayer fluid spacing caused by these cations. Our data are more consistent with a charge neutralization effect wherein the metal ions bind to the inner core, neutralizing negatively charged moieties there. In conjunction with this, Schindler and Osborn (*61*) have noted that the apparent dissociation constant for dissociation of divalent cations from the KDO region of LPS is 14 μM, indicating that such ions bind tightly to the KDO moieties. Moreover, electrostatic double layer theory (*48*) indicates that divalent cations are about 100 times more effective than monovalent cations in lowering the membrane surface potential (ψ_o).

Structure of Liquid-Crystalline LPS Bilayers. The diffraction data show that both Rd (R7) and Rc (SL848) LPS were in a bilayer phase below and above the gel to liquid-crystalline phase transition. The melting of the hydrocarbon chains is evidenced by the change in the wide-angle diffraction from a sharp reflection to a broad band. The disordering of the hydrocarbon chain region is also indicated by the decrease in the repeat period (Table 2). That is, as commonly seen with phospholipids (*30*, *47*, *51*), as the bilayer goes from a gel to a liquid-crystalline phase the area per lipid molecule increases as the hydrocarbon thickness decreases.

To compare the structure of LPS with typical membrane phospholipids in the liquid-crystalline phase, it is useful to determine the area per hydrocarbon chain. As was done for phospholipids (*51*, *63*), we use the area per hydrocarbon chain in the gel phase ($A_g = 20.7$ Å^2, as obtained from the wide-angle diffraction pattern) and the change in hydrocarbon

chain thickness upon melting (as estimated from the difference in lamellar repeat period) to estimate the area per hydrocarbon chain in the liquid-crystalline phase (A_{lc}). For lipids with untilted hydrocarbon chains (such as LPS), the change in area per hydrocarbon chain upon melting (ΔA) can be estimated from the following relation

$$\Delta A = A_g(\Delta V/V_g - \Delta H/H_g)(H_g/H_{lc}) \quad (4)$$

where A is the area per hydrocarbon chain, V is the volume of a hydrocarbon chain, H is the width of the hydrocarbon region, $\Delta A = A_{lc} - A_g$, $\Delta V = V_{lc} - V_g$, and $\Delta H = H_{lc} - H_g$, where the subscripts g and lc represent the gel and liquid-crystalline phases, respectively (*63*). From the electron density profile analysis, $H_g = 35$ Å (see above). If we assume that the 5 Å difference in repeat period observed upon melting (Table 2) were totally due to a difference in hydrocarbon chain thickness of the bilayer, then $H_{lc} = 30$ Å. Although hydrocarbon volumes have not been measured for LPS bilayers, the dilatometry results of Nagle and Wilkinson (*64*, *65*) for the change in volume per methylene group of phospholipids upon chain melting can be used to give estimates for ΔV. For the temperature range used in our experiments, $\Delta V/V_g = 0.072$ for phosphatidylethanolamine (*64*) and $\Delta V/V_g = 0.082$ for phosphatidylcholine (*65*) containing 14 carbons in their hydrocarbon chains. Using these two values for the volume changes upon melting, we obtain A_{lc} values of 25.9 and 26.1 Å^2. We note that these values represent upper estimates for the area per chain in the liquid-crystalline phase, since the calculation was performed using the assumption that the entire change in repeat period was due to a change in hydrocarbon thickness. This is not a bad assumption, since these temperature experiments were performed either in the presence of divalent cations or with high osmotic pressures (log $P = 7.2$). Under these conditions, the apposing bilayers are in steric contact (Figures 2 and 6) so that potential changes in the fluid spacing due to the presence of fluctuation forces in the liquid-crystalline phase are expected to be negligible (*66*). However, if some of the repeat period difference (Table 2) were due to a change in the thickness of the fluid spacing or the saccharide core region, then A_{lc} would be even smaller.

Our calculated A_{lc} value of 26 Å^2 for LPS in the liquid-crystalline phase is comparable to that determined for liquid-crystalline bilayers composed entirely of saturated phosphatidylethanolamine (*51*, *63*). However, 26 Å^2 is quite small compared to hydrocarbon chain areas determined for phospholipids with unsaturated chains typical of phospholipids found in biological membranes, which vary between 32 and 41 Å^2 (*66*−*70*). The relatively small value for A_{lc} in LPS bilayers may be due to several factors, including strong van der Waals attraction between the saturated LPS hydrocarbon chains and possible adhesive interactions between the core sugars from adjacent molecules.

Therefore, the area per hydrocarbon chain is significantly smaller for liquid-crystalline LPS than for typical membrane phospholipids, meaning that the hydrocarbon chains are more tightly packed in LPS bilayers than in phospholipid bilayers. This observation may help to explain the relatively low permeability to hydrophobic molecules that has been observed for the outer membrane of Gram-negative bacteria (*11*).

ACKNOWLEDGMENT

We thank Dr. Joe A. Fralick (Texas Tech University Health Sciences Center) for the generous gift of bacterial strains and Dr. Chris Raetz of the Duke University Medical Center for helpful discussions about the FhuA/LPS crystal structure.

REFERENCES

1. Nikaido, H. (1973) in *Bacterial Membranes and Walls* (Leive, L., Ed.) pp 131−208, Marcel Dekker, New York.
2. Nikaido, H., and Takae, T. (1979) *Adv. Microb. Physiol. 20*, 163−250.
3. Kamio, Y., and Nikaido, H. (1976) *Biochemistry 15*, 2561−2569.
4. Raetz, C. R. H. (1990) *Annu. Rev. Biochem. 59*, 129−170.
5. Stone, R. (1994) *Science 264*, 365−367.
6. Nikaido, H., and Vaara, M. (1985) *Microbiol. Rev. 49*, 1−32.
7. Nikaido, H. (1994) *Science 264*, 382−388.
8. Donaldson, D. M., Roberts, R., Larsen, H. S., and Tew, J. C. (1974) *Infect. Immun. 10*, 657−666.
9. Patterson-Delafield, J., Martinez, R. J., and Lehrer, R. I. (1980) *Infect. Immun. 30*, 180−192.
10. Hancock, R. E. W. (1984) *Annu. Rev. Microbiol. 38*, 237−264.
11. Plesiat, P., and Nikaido, H. (1992) *Mol. Microbiol. 6*, 1323−1333.
12. Roantree, R. J., Kuo, T.-T., and MacPhee, D. G. (1977) *J. Gen. Microbiol. 103*, 223−234.
13. Parker, C. T., Kloser, A. W., Schnaitman, C. A., Stein, M. A., Gottesman, S., and Gibson, B. W. (1992) *J. Bacteriol. 174*, 2525−2538.
14. Fralick, J. A., and Burns-Keliher, L. L. (1994) *J. Bacteriol. 176*, 6404−6406.
15. Stan-Lotter, H., Gupta, M., and Sanderson, K. E. (1979) *Can. J. Microbiol. 25*, 475−485.
16. Hiruma, R., Yamaguchi, A., and Sawai, T. (1984) *FEBS Lett. 170*, 268−272.
17. Takayama, K., Din, Z. Z., Mukerjee, P., Cooke, P. H., and Kirkland, T. N. (1990) *J. Biol. Chem. 265*, 14023−14029.
18. Shnyra, A., Hultenby, K., and Lindberg, A. A. (1993) *Infect. Immun. 61*, 5351−5360.
19. Brandenburg, K., Mayer, H., Koch, M. H. J., Weckesser, J., Rietschel, E. T., and Seydel, U. (1993) *Eur. J. Biochem. 218*, 555−563.
20. Takayama, K., Mitchell, D. H., Din, Z. Z., Mukerjee, P., Li, C., and Coleman, D. L. (1994) *J. Biol. Chem. 269*, 2241−2244.
21. Seydel, U., Brandenburg, K., Koch, M. H. J., and Rietschel, E. T. (1989) *Eur. J. Biochem. 186*, 325−332.
22. Naumann, D., Schultz, C., Sabisch, A., Kastowsky, M., and Labischinski, H. (1989) *J. Mol. Struct. 214*, 213−246.
23. Seydel, U., Koch, M. H. J., and Brandenburg, K. (1993) *J. Struct. Biol. 110*, 232−243.
24. Labischinski, H., Barnickel, G., Bradaczek, H., Nauman, D., Rietschel, E. T., and Giesbrecht, P. (1985) *J. Bacteriol. 162*, 9−20.
25. Labischinski, H., Naumann, D., Schultz, C., Kusumoto, S., Shiba, S., Rietschel, E. T., and Giesbrecht, P. (1989) *Eur. J. Biochem. 179*, 659−665.
26. Kastowsky, M., Gutberlet, T., and Bradaczek, H. (1993) *Eur. J. Biochem. 217*, 771−779.
27. Kastowsky, M. (1993) in *Bacterial Endotoxin: Recognition and Effector Mechanisms* (Levin, J., Alving, C. R., Munford, R. S., and Stutz, P. L., Eds.) pp 61−72, Excerpta Medica, Amsterdam.
28. Moody, M. F. (1963) *Science 142*, 1173−1174.
29. Worthington, C. R., King, G. I., and McIntosh, T. J. (1973) *Biophys. J. 13*, 480−494.
30. McIntosh, T. J., and Simon, S. A. (1986) *Biochemistry 25*, 4058−4066.
31. Galanos, C., Luderitz, O., and Westphal, O. (1969) *Eur. J. Biochem. 9*, 245−249.

32. Qureshi, N., Takayama, K., Heller, D., and Fenselau, C. (1983) *J. Biol. Chem. 258*, 12947−12951.
33. LeNeveu, D. M., Rand, R. P., Parsegian, V. A., and Gingell, D. (1977) *Biophys. J. 18*, 209−230.
34. Parsegian, V. A., Fuller, N., and Rand, R. P. (1979) *Proc. Natl. Acad. Sci. U.S.A. 76*, 2750−2754.
35. McIntosh, T. J., Magid, A. D., and Simon, S. A. (1987) *Biochemistry 26*, 7325−7332.
36. Brandenburg, K., and Seydel, U. (1984) *Biochim. Biophys. Acta 775*, 225−238.
37. Parsegian, V. A., Rand, R. P., Fuller, N. L., and Rau, R. C. (1986) *Methods Enzymol. 127*, 400−416.
38. McIntosh, T. J., Magid, A. D., and Simon, S. A. (1989) *Biochemistry 28*, 17−25.
39. O'Brien, F. E. M. (1948) *J. Sci. Instrum. 25*, 73−76.
40. Weast, R. C. (1984) *Handbook of Chemistry and Physics*, p E-42, CRC Press, Boca Raton, FL.
41. McIntosh, T. J., and Holloway, P. W. (1987) *Biochemistry 26*, 1783−1788.
42. Blaurock, A. E., and Worthington, C. R. (1966) *Biophys. J. 6*, 305−312.
43. Herbette, L., Marquardt, J., Scarpa, A., and Blasie, J. K. (1977) *Biophys. J. 20*, 245−272.
44. Shannon, C. E. (1949) *Proceedings of the Institution of Radio Engineers of New York 37*, 10−21.
45. Sayre, D. (1952) *Acta Crystallogr. B5*, 843.
46. McIntosh, T. J., Simon, S. A., Needham, D., and Huang, C.-h. (1992) *Biochemistry 31*, 2020−2024.
47. Tardieu, A., Luzzati, V., and Reman, F. C. (1973) *J. Mol. Biol. 75*, 711−733.
48. Israelachvili, J. N. (1992) *Intermolecular and Surface Forces*, pp 231−246, Academic Press, London.
49. Lesslauer, W., Cain, J. E., and Blasie, J. K. (1972) *Proc. Natl. Acad. Sci. U.S.A. 69*, 1499−1503.
50. Janiak, M. J., Small, D. M., and Shipley, G. G. (1979) *J. Biol. Chem. 254*, 6068−6078.
51. McIntosh, T. J., and Simon, S. A. (1986) *Biochemistry 25*, 4948−4952.
52. Brandenburg, K. (1993) *Biophys. J. 64*, 1215−1231.
53. Ferguson, A. D., Hofmann, E., Coulton, J. W., Diederichs, K., and Welte, W. (1998) *Science 282*, 2215−2220.
54. Din, Z. Z., Mukerjee, P., Kastowsky, M., and Takayama, K. (1993) *Biochemistry 32*, 4579−4586.
55. McIntosh, T. J., and Simon, S. A. (1994) *Biochemistry 33*, 10477−10486.
56. Klibanov, A. L., Maruyama, K., Torchilin, V. P., and Huang, L. (1990) *FEBS Lett. 268*, 235−237.
57. Papahadjopoulos, D., Allen, T. M., Gabizon, A., Mayhew, E., Matthay, K., Huang, S. K., Lee, K.-D., Woodle, M. C., Lasic, D. D., Redemann, C., and Martin, F. J. (1991) *Proc. Natl. Acad. Sci. U.S.A. 88*, 11460−11464.
58. Needham, D., McIntosh, T. J., and Lasic, D. D. (1992) *Biochim. Biophys. Acta 1108*, 40−48.
59. Needham, D., Stoicheva, N., and Zhelev, D. V. (1997) *Biophys. J. 73*, 2615−2629.
60. Kenworthy, A. K., Hristova, K., Needham, D., and McIntosh, T. J. (1995) *Biophys. J. 68*, 1921−1936.
61. Schindler, M., and Osborn, M. J. (1979) *Biochemistry 18*, 4425−4430.
62. Jou, R., and Cowan, J. A. (1991) *J. Am. Chem. Soc. 113*, 6686−6687.
63. Nagle, J. F., and Wiener, M. C. (1988) *Biochim. Biophys. Acta 942*, 1−10.
64. Wilkinson, D. A., and Nagle, J. F. (1981) *Biochemistry 20*, 187−192.
65. Nagle, J. F., and Wilkinson, D. A. (1978) *Biophys. J. 23*, 159−175.
66. McIntosh, T. J., Advani, S., Burton, R. E., Zhelev, D. V., Needham, D., and Simon, S. A. (1995) *Biochemistry 34*, 8520−8532.
67. Lis, L. J., McAlister, M., Fuller, N., Rand, R. P., and Parsegian, V. A. (1982) *Biophys. J. 37*, 657−666.
68. McIntosh, T. J., and Magid, A. D. (1993) in *Phospholipid Handbook* (Cevc, G., Ed.) pp 553−577, Marcel Dekker, New York.
69. Petrache, H. I., Tristram-Nagle, S., and Nagle, J. F. (1998) *Chem. Phys. Lipids 95*, 83−94.
70. Tristram-Nagle, S., Petrache, H. I., and Nagle, J. F. (1998) *Biophys. J. 75*, 917−925.

BI990867D